SHAN, Kui; WANG, Shengwei; ZHUANG, Chaoqun. Controlling a large constant speed centrifugal chiller to provide grid frequency regulation: A validation based on onsite tests. Applied Energy, 2021, 300: 117359.

https://doi.org/10.1016/j.apenergy.2021.117359 **This is the Pre-Published Version.**

Controlling a Large Constant Speed Centrifugal Chiller to Provide Grid Frequency Regulation: A Validation Based on Onsite Tests

Kui Shan[1,2], Shengwei Wang[2,1], Chaoqun Zhuang[2]

1 Research Institute for Smart Energy, The Hong Kong Polytechnic University

2 Department of Building Services Engineering, The Hong Kong Polytechnic University

Abstract:

High penetration of intermittent renewables may cause safety and stability problems to the electricity grid. Building thermal loads could contribute to the grid stability in the era of renewable energy and smart grid, because they are high and flexible. This study proposes a model predictive control strategy to control a large constant speed centrifugal chiller to follow grid frequency regulation signals while providing sufficient cooling to the building. Onsite tests were conducted to identify critical parameters in the process including time delay and ramping speed of chiller power consumption. A dynamic platform was built based on the studied system and fine-tuned using onsite tests data. Validation tests were conducted using the 40 minutes Regulation A and Regulation D test signals provided by PJM (Pennsylvania - New Jersey - Maryland Interconnection). According to the onsite tests, the total delay time and the maximum ramping speed of chiller power were 20–25 seconds and 2.53 kW/s, respectively. Validation based on the 40 minutes test signals shown that the composite performance scores were 0.901 and 0.885 for Regulation A test and Regulation D test, respectively. Continuous 12 hours validation tests in a working day shown that the composite scores were 0.917 and 0.893 for Reg A and Reg D tests, respectively. And the studied constant speed centrifugal chiller could provide a regulation capacity of 5%-7.5% of its nominal power.

Key words: grid frequency regulation; ancillary service; grid-responsive building; demand response; chiller; HVAC

The short version of the paper was presented at ICAE2020, Dec 1-10, 2020. This paper is a substantial extension of the short version of the conference paper.

Nomenclature:

English symbols

a,b,c	empirical coefficients
B	the ratio of the impeller channel depth at the intake to that at exhaust
c_{r2}	impeller exit radial velocity (m/s)
$c_{imp,ext}$	the vapor velocity at the impeller exhaust (m/s)
c_p	the specific heat of water (kJ/(kg·K))
CAP_{flow}	the thermal capacity (kJ/K)
C_{reg}	regulation capacity (kW)
G	global solar radiation (W/m^2)
H	compressor head, loss, or pression work (kW/kg),
m	mass flow (kg/s)
P_{ch}	Power consumption of the chiller (kW)
$P_{ch,up,sp}$	Power consumption upper limit set-point of the chiller (kW)
P_{inter}	internal compression power (kW)
P_{loss}	constant part of power losses (kW)
P_{tar}	target power consumption (kW)
P_{ref}	reference power (kW)
Q_{load}	cooling load (kW)
Q_{meas}	the current measured building cooling load (kW)
Q_N	nominal capacity of chillers (kW)
Q_{pred}	the predicted cooling load (kW)
S_{reg}	regulation signal
T	Temperature (°C)
T'	the temperature after introducing dynamic effects (°C)
T_{wevout}	Supply chilled water temperature (°C)
$T_{wevout,sp}$	Supply chilled water temperature set-point (°C)
$T'_{wevout,sp}$	optimal chilled water temperature set-point (°C)
$T''_{wevout,sp}$	calculated empirical optimal set-point (°C)
$T_{wevout,sp,min}$	the allowed minimum supply chilled water temperature (°C)
u_2	the impeller tip speed (m/s)
υ_{in}	the specific volumes at the impeller intake (m^3)
υ_{ext}	the specific volumes at the impeller exhaust (m^3)
V	volume (m^3)

Greek symbols

α	multiple linear regression coefficients
β	the chiller vane angle
γ	the pre-rotation vane angle
ζ	multiple linear regression coefficients
ρ	density (kg/m^3)
ς, ψ_1, ψ_2, χ	constants
τ	Time (s)

Subscripts

com	compressor
cd	condenser
ev	evaporator

The short version of the paper was presented at ICAE2020, Dec 1-10, 2020. This paper is a substantial extension of the short version of the conference paper.

hyd	hydrodynamic losses
imp	impeller
oa	outdoor air
pol	polytropical
pred	predicted
in	inlet
rtn	return
sup	supply
th	theoretical, threshold
w	water

Abbreviations

AGC	Automatic Generation Control
AHU	Air Handling Units
COP	Coefficient Of Performance
HVAC	Heating, Ventilation and Air Conditioning
PJM	Pennsylvania - New Jersey - Maryland Interconnection
PLR	part load ratio
VSD	Variable Speed Drivers

1 Introduction

Renewable energy is projected to reach 40% of the global grid power generation in the 2040s [1]. Wind and solar power installation capacity is expected to be 36% by 2030 in India [2], and 60% by 2050 in China [3]. However, the high penetration of such intermittent renewables would put high stress on the stability and safety operation of the grid [2][4]. Large amount of renewable energy has been curtailed for grid stability. For instance, the lost sales for wind power producers accounted to 18.7 billion RMB (2.7 billion USD) in 2016 in China [5].

The supply and demand side of the grid must always be balanced. Grid frequency is regulated to 50 Hz or 60 Hz. It indicates the balance between supply and demand. Downward deviation means electricity supply is less than demanded, and upward deviation means the supply is higher than demanded. As one of the two types of ancillary services, frequency regulation (the other type is called reserves) is to balance small mismatches between load and generation. It is conventionally done by regulating the electricity supply and relies on system inertia provided by the rotary of thermal power generators and turbines. The percentage of such system inertia

The short version of the paper was presented at ICAE2020, Dec 1-10, 2020. This paper is a substantial extension of the short version of the conference paper.

is declining with the increase of renewables, making conventional method difficult to fulfil the task [2][6].

Demand side has recently shown its high potential in grid frequency regulation. Buildings consume over 90% of electricity in Hong Kong, and 75% in the United States [7]. In summer peak load period, air-conditioning systems may consume over 1/3 of the total electricity power generation [8]. Fortunately, building thermal loads are flexible, particularly when a building is equipped with thermal storage systems [9][10]. Also, building thermal equipment can response quickly to grid frequency regulation signals [11].

Many researchers have studied demand side frequency regulation [12][13]. Commercial building HVAC (Heating, Ventilation and Air Conditioning) fans are the most extensively studied equipment for frequency regulation because their power could be easily and quickly adjusted by VSDs (Variable Speed Drivers). A study on supply air duct and fans estimated that at least 4 GW regulation reserve capacity could be provided by commercial buildings in US [14]. Another study on AHU fans compared two control methods, i.e. adjust duct pressure set-point and adjust zone temperature set-point. It was found that the zone temperature reset method was more effective [15]. A feedforward control architecture was proposed to control the fan speed in commercial buildings. Results shown that a single 35 kW fan could provide about 5 kW (14.3%) regulation capacity [16][17]. A hierarchical control approach has been proposed to control HVAC fan to follow fast changing regulation signals, and has been tested in a commercial building [18][19]. A dynamic VAV (Variable Air Volume) system model has been developed to simulate the provision of grid frequency regulation. Tests results shown that damper positions of terminal units affected the ancillary control performance significantly [20]. Residential ventilation fans were proposed to provide ancillary services through aggregation [21]. IT and cooling systems in data centers have also been investigated for frequency regulation [22][23].

The short version of the paper was presented at ICAE2020, Dec 1-10, 2020. This paper is a substantial extension of the short version of the conference paper.

Chiller COP could be exploited for extra flexibility, according to a study on providing frequency regulation using building thermodynamics and HVAC system [24]. Another study on the use of chiller and AHU (Air Handling Unit) fan for ancillary services got similar conclusions. The simulation study adopted a chiller power model based on a constant chiller efficiency and an estimated time delay of 30 seconds [25][26]. However, quasi-steady-state HVAC models do not capture system dynamics during regulation control, and the regulation capacity could be significantly overestimated [27]. A regulation capacity reset strategy has been developed and tested on a split system heat pump and an RTU (rooftop unit). The daily cost saving for regulation control was estimated to be around 12%–26%. It was also concluded that HVAC equipment can outperform batteries for frequency regulation [27][28]. A method has been developed for using VSD chillers for frequency regulation. It was successfully tested on a chiller with two identical VSD compressors rated at 60 kW each. The performance scores were 0.89 for Regulation A and 0.86 for Regulation D while providing 15 kW regulation capacity [29][30].

According to the literature survey presented above, the research on the use of large constant speed centrifugal chillers for frequency regulation is still missing. Constant speed chillers are widely installed. They do not require VSDs which often consume 4%–8% of the converted energy for operation [31][32]. They have higher efficiency in full load conditions, and their maintenance is easier. Furthermore, very few studies have conducted onsite tests on the time delay when using chillers for frequency regulation, though it is time-sensitive [33]. This study targets at discovering the potential of exploiting constant speed chillers for higher frequency regulation capacity.

Contributions of this work include: (1) This study provides a first try on the use of a large and constant speed centrifugal chiller for grid frequency regulation. (2) A new and practically effective control strategy is developed to regulate chiller inlet guide vane opening for chiller

The short version of the paper was presented at ICAE2020, Dec 1-10, 2020. This paper is a substantial extension of the short version of the conference paper.

power control. (3) Onsite tests were conducted to discover the essential parameters during the provision of frequency regulation, i.e., time delay and ramping speed of chiller power consumption. The onsite test results were used to fine-tune the dynamic simulation platform built based on the real system. Onsite tests and dynamic validation results were analyzed and discussed.

The remaining of this paper is organized as follows: section 2 describes the proposed control strategy for using a constant speed centrifugal chiller for frequency regulation. Section 3 presents the validation platforms, including the real chiller plant, and the dynamic simulation platform. Section 4 demonstrates the onsite and dynamic tests results, as well as discussions. Section 5 presents conclusions.

2 The proposed control strategy

2.1 PJM regulation signals

Before describing the control strategy, it is necessary to introduce the frequency regulation program. This study is based on the program provided by PJM market. Two different types of regulation signals are generated for different kinds of regulation resources, i.e. the slower varying Regulation A signal (RegA) and the faster varying Regulation D signal (RegD). These two signals cooperate with each other to match the regulation needs of the grid system. RegA is a conventional signal meant to recover larger, longer fluctuations in system conditions, while RegD is a dynamic signal that requires resources to respond almost instantaneously [34]. Both RegA and RegD signals range from -1 to 1 and are updated every 2 seconds.

When providing frequency regulation, the target power consumption could be calculated by Eq. (1). It varies rapidly between $P_{ref} - C_{reg}$ and $P_{ref} + C_{reg}$.

$$P_{tar} = P_{ref} + C_{reg} \cdot S_{reg} \quad (1)$$

The short version of the paper was presented at ICAE2020, Dec 1-10, 2020. This paper is a substantial extension of the short version of the conference paper.

where, P_{tar} is the target power consumption (kW). P_{ref} is the reference power defined as the average of the minimum and maximum power consumption (kW). C_{reg} is the regulation capacity (kW), which is the difference between maximum unit power consumption and the reference power. S_{reg} is the regulation signal. The regulation capacity and the reference power should be dynamically reset an hour-ahead.

A performance score is calculated hourly by PJM to evaluate the regulation credit. It reflects the accuracy of regulation resources in following AGC (Automatic Generation Control) signal. The composite performance score is an average of three sub-scores, i.e. the accuracy score, the delay score, and the precision score. Detailed calculation method of the performance score is documented in PJM manual [34]. A resource can only get certificated by PJM after achieving three consecutive scores of 0.75 or above.

2.2 The proposed control method for using constant centrifugal chillers for frequency regulation

Centrifugal chillers are widely used for large buildings, factories or even districts for space cooling. The power consumption of chillers could account for about 40% of the total HVAC system consumption. The amount of cooling provided by the chillers should be controlled in response to the varying cooling load which changes with weather condition, occupancy usage, etc. At system level, the capacity of the chiller plant could be roughly controlled by sequencing of multiple chillers [35]. At component level, the capacity control methods of a single centrifugal chiller can be achieved in three common ways [36]: (a) use inlet guide vane; (b) use VSD; (c) use hot gas bypass valve.

The concepts of these methods are almost the same: control the capacity of chillers by changing the refrigerant flow through the evaporator where cooling effect is generated. When method (a) is used, the refrigerant gas entry angle to the compressor impeller changes with the change of inlet guide vane openings. The refrigerant flow is therefore changed as the vane opening

The short version of the paper was presented at ICAE2020, Dec 1-10, 2020. This paper is a substantial extension of the short version of the conference paper.

changes. When method (b) is used, the refrigerant flow is changed by varying motor speed of the compressor. When method (c) is used, part of the hot refrigerant gas from compressor discharge port is recirculated back into the evaporator. The amount of bypassed refrigerant is controlled by a hot gas bypass valve. This method should be avoided whenever possible, because the bypassed refrigerant has already consumed electricity but generates no cooling effect. It is primary used for protecting compressors in low load conditions.

The control strategy proposed in this study aims to use a large and constant speed centrifugal chiller to provide frequency regulation. More specifically, the objective is to control the chillers instantaneous power consumption according to grid frequency regulation signals while still fulfilling the demanded cooling supply. When the compressor inlet guide vane opening is adjusted, the power consumption and the cooling capacity will be changed. Therefore, it is proposed to regulate the inlet guide vane opening according to the grid frequency regulation signals. Meanwhile, the building thermal environment will only be affected slightly due to the thermal buffer effect of the cooling delivery system and building thermal mass.

The constant speed chiller receives two settings from the building automation system. One is the supply chilled water temperature set-point, the other is the chiller power consumption upper limit set-point. In normal operation, the internal controller controls the opening of compressor inlet guide vane to achieve the supply chilled water temperature set-point. The chiller power consumption upper limit is mainly used to avoid too high chiller current during chiller starting period, or to limit peak demand in special occasions [36].

The proposed strategy only considers one chiller in operation. Fig. 1 shows the local chiller control in the proposed control strategy. The local control loop coordinates two PID (Proportional–Integral–Derivative) controllers. One is to control the supply chilled water temperature, the other is to constrain the chiller power consumption not exceed the upper limit

The short version of the paper was presented at ICAE2020, Dec 1-10, 2020. This paper is a substantial extension of the short version of the conference paper.

set-point. The control signals from the two controllers are compared and the lower one is used to command the compressor inlet guide vane.

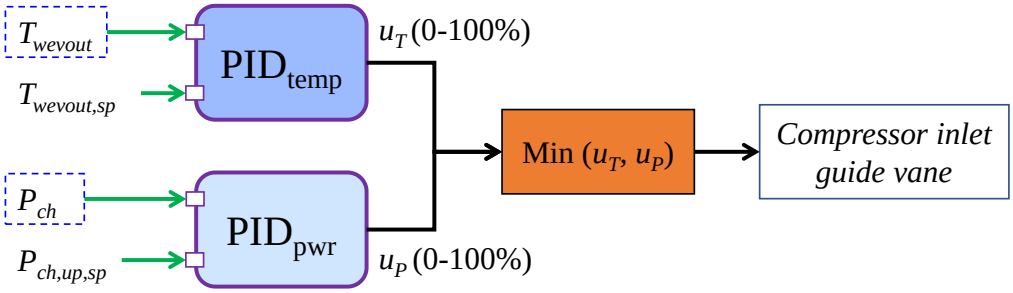

where, T_{wevout} is the supply chilled water temperature (℃), $T_{wevout,sp}$ is the supply chilled water temperature set-point (℃). P_{ch} is the power consumption of the chiller (kW). $P_{ch,up,sp}$ is the power consumption upper limit set-point of the chiller (kW).

Fig. 1 Schematic of local chiller control in the proposed control strategy

The $T_{wevout,sp}$ and $P_{ch,up,sp}$ are two critical set-points in the whole control strategy. Fig. 2 demonstrates the determination process of the two set-pints. The left side of the figure shows the process for determining the $P_{ch,up,sp}$, and the right side of the figure shows the process for determining the $T_{wevout,sp}$. The reference power (P_{ref}) and regulation capacity (C_{reg}) are firstly determined based on the predicted building cooling load and chiller efficiency. The building load in the next hour is predicted by a previously developed multiple linear regression model based on real time operation data and real time working conditions, as shown in Eq. (2) [36]. The model is trained using operation history data and is adaptive to the system because it is periodically updated online. The cooling load in the future hour is assumed to be related with current load, outdoor air temperature, solar radiation, and other time related factors including occupancy number. Those time related factors are considered in time-of-day. The time-of-day is evenly divided into 24 time slots (each slot is one hour), each is multiplied by a numerical value.

The short version of the paper was presented at ICAE2020, Dec 1-10, 2020. This paper is a substantial extension of the short version of the conference paper.

$$Q_{pred} = \alpha_0 + \alpha_1 \cdot Q_{meas} + \alpha_2 \cdot T_{oa} + \alpha_3 \cdot G + [\zeta_0\ \zeta_1 \dots \zeta_{23}] \begin{bmatrix} a_0 \\ a_1 \\ \dots \\ a_{23} \end{bmatrix} \quad (2)$$

where, Q_{pred} is the predicted cooling load in the next hour (kW). α and ζ are multiple linear regression coefficients to be determined based on real data ($\alpha_0: kW$, $\alpha_1: kW/kW$, $\alpha_2: kW/℃$, $\alpha_3: kW/(W/m^2)$, $\zeta: kW$). Q_{meas} is the current measured building cooling load (kW). T_{oa} and G are current outdoor air temperature (°C) and global solar radiation (W/m^2), respectively. Both are obtained online from Hong Kong Observatory. a_0, a_1, …, a_{23} represent the current time slot, and is either 0 or 1. For instance, if the current time is between 02:00 am and 03:00 am, then a_2 is 1 and all others are 0.

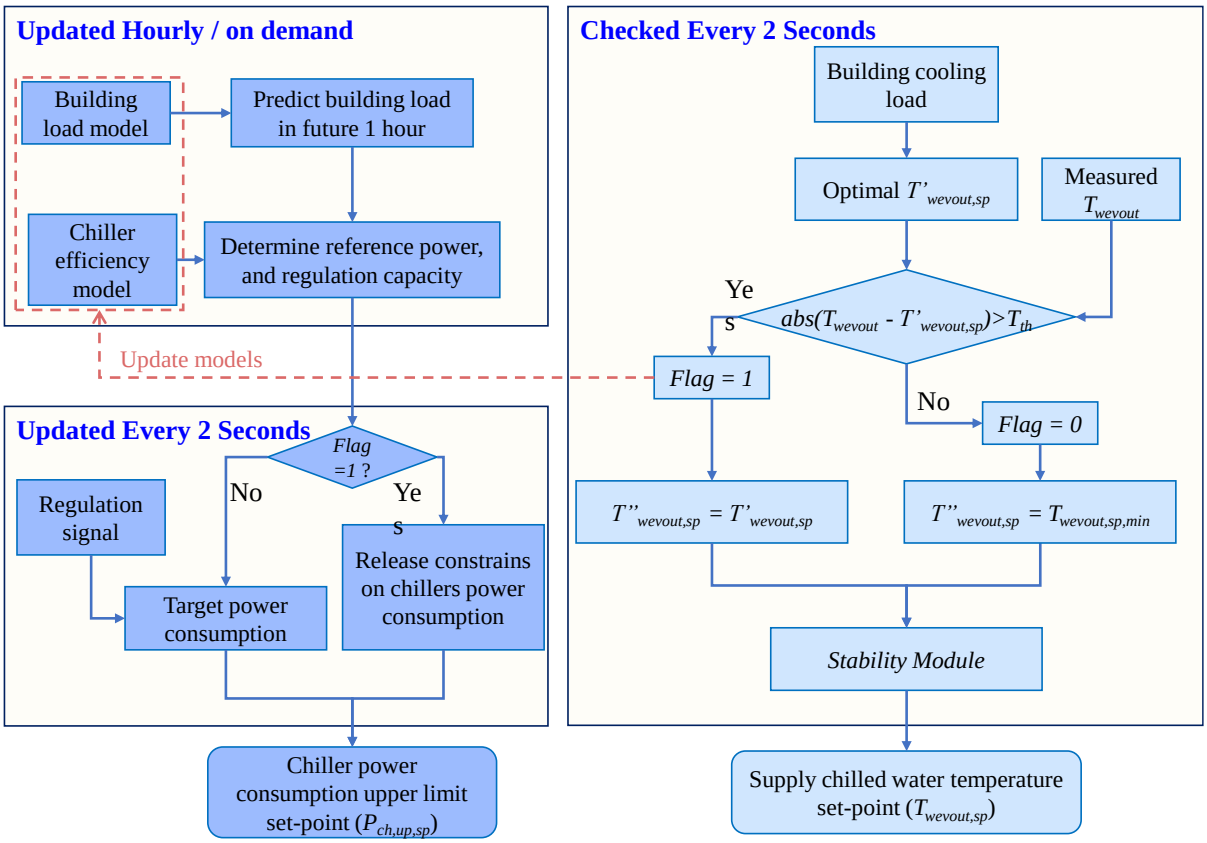

Fig. 2 Determination of the two critical set-points in the control strategy

After the building load is predicted, the chiller power consumption in the future hour could be estimated based on the chiller efficiency model (Eq. (3-4)). The chiller power consumption is

The short version of the paper was presented at ICAE2020, Dec 1-10, 2020. This paper is a substantial extension of the short version of the conference paper.

estimated by a polynomial fit of the part load ratio (PLR), which is the ratio of actual chiller load to nominal chiller capacity. The reference power is determined to be the mean of predicted chiller power consumption in the future one hour, and the regulation capacity is determined to be 5% of the reference power.

$$PLR = {Q_{pred}}/{Q_N} \tag{3}$$

$$P_{ch,pre} = c_0 + c_1 \cdot PLR + c_2 \cdot PLR^2 \tag{4}$$

$$T'_{wevout,sp} = a + b \cdot Q_{meas} \tag{5}$$

where, *PLR* is the chiller part load ratio, which is the predicted building load (Q_{pred}: kW) divided by the nominal capacity of chillers (Q_N: kW). $P_{ch,pre}$ is the predicted chiller power consumption (kW). c_0, c_1, and c_2 are empirical coefficients to be trained using history data (kW). a and b are empirical coefficients (a: ℃, b: ℃ /kW). $T'_{wevout,sp}$ is the optimal chilled water temperature set-point (°C).

The chiller power consumption upper limit set-point is the target power consumption (P_{tar}) computed by Eq.(1). However, if the supply chilled water temperature is too high (as indicated by an internal parameter named "*Flag*" in the flow chart), the constraints on chillers power consumption have to be released.

In the process of determining the supply chilled water temperature set-point, the proposed strategy also tries to minimize the total power consumption of chillers and chilled water pumps by optimizing the temperature set-point. The optimal set-point is determined by an empirical equation (Eq. (5)) based on the measured actual building cooling load and constrained between a reasonable range (5 ℃ - 9 ℃). Higher cooling load often means lower optimal chilled water temperature set-point. The empirical optimal set-point is then compared with the actual measured supply chilled water temperature. If the measured value is higher than the optimal value for a certain amount (a threshold T_{th}), the internal value "*Flag*" is set to 1 and the

The short version of the paper was presented at ICAE2020, Dec 1-10, 2020. This paper is a substantial extension of the short version of the conference paper.

uncorrected set-point ($T''_{wevout,sp}$) is the calculated empirical optimal set-point. Otherwise, the "*Flag*" is set to 0 and the uncorrected set-point is the allowed minimum supply chilled water temperature ($T_{wevout,sp,min}$), and the chiller will be controlled to follow frequency regulation signals. To avoid rapid fluctuation in the final set-points, the stability module adopts a filter previously developed based on weighted moving average and three-sigma rule (i.e. empirical rule) [37].

It should be noticed that the determination of chiller power consumption upper limit set-point is the functional part of following the regulation signals. The right-side part in Fig. 2 guarantees the required building thermal environment beside of resetting supply chilled water temperature. If "*Flag*" is determined to be 1, it means there is a risk to compromise the building thermal environment. Since the priority is given to building thermal environment, the constraint on chiller power consumption will be released to provide more cooling. In the meantime, the building load model and the chiller efficiency model will be updated.

3 Validation platform

This study is conducted based on the HVAC system for a real high-rise commercial building in Hong Kong. The critical parameters were discovered via onsite tests, and the proposed control strategy were validated on a dynamic simulation platform built based on a real system and onsite data. This section presents the real system and the dynamic platform.

3.1 The real chiller plant

The chiller plant consists of six identical large constant speed centrifugal chillers. Table 1 shows the nameplate parameters of the chillers. Each chiller is associated with a chilled water pump and a cooling water pump. Both two types of the pumps are constant speed and their on/off are interlocked with the on/off status of chillers.

Table 1 Critical parameters in the specification of the large chillers

The short version of the paper was presented at ICAE2020, Dec 1-10, 2020. This paper is a substantial extension of the short version of the conference paper.

Cooling Capacity	Rated Current	Entering Temp.	Leaving Temp.	Flow Rate	Pressure Drop	Connection Size
		Evaporator				
7230 kW	75 A	10.5 °C	5.5 °C	345 L/s	110 kPa	450 mm
Refrigerant	Power Source	Condenser				
R134a	11 kV 50 Hz/3 phase	32 °C	37 °C	410 L/s	110 kPa	500 mm

3.2 The dynamic simulation platform and the models used

Fig. 3 demonstrates the framework of the dynamic simulation platform built using the software Trnsys 18 [38]. The platform mainly consists of a chiller model, a building model, a thermal buffer model, and a controller module. The detailed chiller model simulates the instantaneous cooling capacity and power consumption based on these input variables, including the inlet water temperatures and flow rates of condenser and evaporator. The building model gets the cooling load from a data file which stores the selected historical cooling load of the studied real building and calculates the return chilled water temperature. The thermal buffer model is used to simulate the thermal buffer effect of the cooling delivery system and building mass. The proposed control strategy is programed in Matlab™ and called by Type 155 from Trnsys 18.

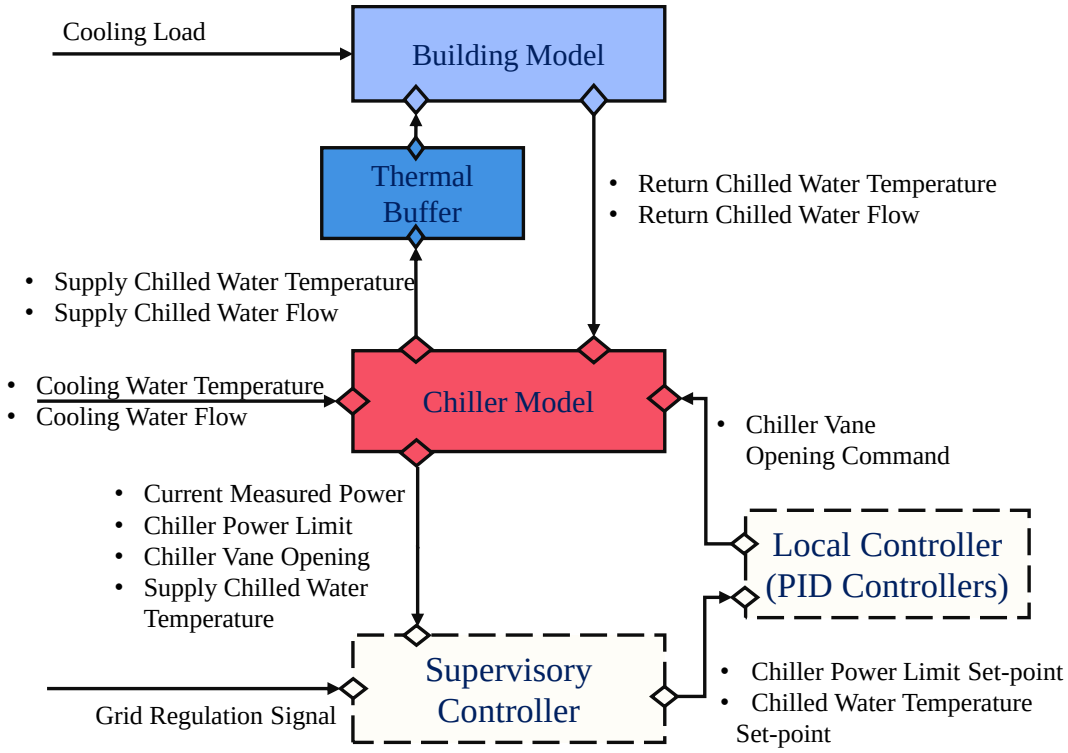

The short version of the paper was presented at ICAE2020, Dec 1-10, 2020. This paper is a substantial extension of the short version of the conference paper.

Fig. 3 Framework of the dynamic simulation platform

Chiller model

A previously developed dynamic chiller model was used to simulate the chiller dynamic performance under various working conditions. The mean relative difference between the simulated and measured chiller capacity is 10.8%, and the mean relative difference between the simulated and measured chiller power is 6.0% [35][39]. The model is based on impeller tip speed, impeller exhaust area, impeller blades angle and 13 coefficients/parameters. The compression process in the compressor, the heat transfer process in the evaporator and the condenser are simulated. The compressor model is based on the Euler turbo-machine equation (Eq. (6) [35][39]), mass conversion equation, and energy balance equation. Eqs. (7–8) [35][39] describe the energy balances in the compressor control volume and the impeller control volume. Eqs. (9–10) [35][39] show the hydrodynamic losses (flow friction losses, inlet losses and incidence losses) in the two control volumes ($H_{hyd,com}$ and $H_{hyd,imp}$).

$$H_{th} = u_2\left[u_2 - \left(\frac{\pi^2}{8}\right)^2 c_{r2}\left(ctg\beta + B\frac{\upsilon_{in}}{\upsilon_{ext}}tg\gamma\right)\right] \tag{6}$$

$$H_{th} = H_{pol,com} + H_{hyd,com} \tag{7}$$

$$H_{th} = H_{pol,imp} + H_{hyd,imp} + \frac{c^2_{imp,ext}}{2} \tag{8}$$

$$H_{hyd,com} = \varsigma\left[1 + \psi_1\left(\frac{\upsilon_{in}}{\upsilon_{ext}}\frac{1}{\cos\gamma}\right)^2 + \psi_2\left(\frac{\upsilon_{in}}{\upsilon_{ext}}tg\gamma\right)^2\right]c^2_{r2} \tag{9}$$

$$H_{hyd,imp} = \varsigma\left[\chi + \psi_1\left(\frac{\upsilon_{in}}{\upsilon_{ext}}\frac{1}{\cos\gamma}\right)^2 + \psi_2\left(\frac{\upsilon_{in}}{\upsilon_{ext}}tg\gamma\right)^2\right]c^2_{r2} \tag{10}$$

where H_{th} is the compressor theoretical head (kW/kg), H_{hyd} is the hydrodynamic losses (kW/kg), H_{pol} is the polytropical compression work (kW/kg), u_2 is the impeller tip speed (m/s), c_{r2} is impeller exit radial velocity (m/s), β is the vane angle, γ is the pre-rotation vane angle, B is the

The short version of the paper was presented at ICAE2020, Dec 1-10, 2020. This paper is a substantial extension of the short version of the conference paper.

ratio of the impeller channel depth at the intake to that at exhaust, υ_{in} and υ_{ext} are the specific volumes at the impeller intake and exhaust, respectively (m^3), $c_{imp,ext}$ is the vapor velocity at the impeller exhaust (m/s), and ς, ψ_1, ψ_2, χ are the introduced constants. Subscripts *com* and *imp* indicate compressor and impeller, respectively.

The chiller power is calculated using Eq. (11) [35][39], which is based on the internal compression power (P_{inter}*:* kW) and a constant leakage ratio. First part of the equation ($c \cdot P_{inter}$) represents the driving power and variable part of power loss with a coefficient c, while the second part (P_{loss}*:* kW) represents constant part of power losses.

$$P_{ch} = c \cdot P_{inter} + P_{loss} \tag{11}$$

The classical heat exchanger efficiency method is used to simulate the heat transfer processes in the evaporator and the condenser. Two thermal storage units are used to simulate the chiller dynamic responses to the changes of inlet temperatures. Eqs. (12–13) [35][39] show the first-order differential models of the two heat exchangers. Left-hand side of both equations indicate the energy increase in the control volume, and right-hand side indicate net inlet energy.

$$CAP_{flow,ev} \frac{dT'_{ev,in}}{d\tau} = c_p M_{w,ev} \left(T_{ev,in} - T'_{ev,in} \right) \tag{12}$$

$$CAP_{flow,cd} \frac{dT'_{cd,in}}{d\tau} = c_p M_{w,cd} \left(T_{cd,in} - T'_{cd,in} \right) \tag{13}$$

where CAP_{flow} is the thermal capacity (kJ/K), T is the temperature (℃), T' is the temperature after introducing dynamic effects (℃), c_p is the specific heat of water (kJ/(kg·K)), subscript *"ev"* indicates evaporator, subscript *"cd"* indicates condenser and subscript *"in"* indicates inlet.

Thermal buffer model

The thermal buffer model is used to calculate the supply chilled water temperature to the building. A virtual water storage tank is used to simulate the thermal buffer effect. Eq. (14)

The short version of the paper was presented at ICAE2020, Dec 1-10, 2020. This paper is a substantial extension of the short version of the conference paper.

shows the energy balance of this virtual water storage tank. Left-hand side of the equation indicates the energy increase in the thermal buffer, and right-hand side indicates net energy flow into the buffer.

$$c_p \cdot \rho \cdot V \cdot \frac{d_T}{d_\tau} = c_p \cdot \left(T_{wevout} - T_{sup}\right) \cdot m_{wev} \quad (14)$$

where, ρ is water density (kg/m^3). V is the volume of the virtual water tank (m^3). T is the average temperature of water in the tank (℃). τ is time (s). T_{wevout} is the inlet water temperature of the virtual tank (℃). T_{sup} is the outlet water temperature of the virtual tank, or supply chilled water temperature to the building (℃). m_{wev} is the mass flow rate of water goes through the virtual tank (kg/s).

Building model and return chilled water temperature

The real cooling load of the studied building is adopted in the platform. The recorded history cooling data is stored in a txt file and imported to the dynamic platform by using Type 9e in Trnsys 18. The building model computes return chilled water temperature from the building based on thermal energy balance, as shown in Eq. (15).

$$T_{rtn} = T_{sup} + Q_{load}/\left(c_p \cdot m_{wev}\right) \quad (15)$$

4 Test results and discussions

Onsite tests were firstly conducted to discover the critical parameters of chillers when providing frequency regulation. The parameters were then used to fine tune the dynamic platform for the validation of the proposed control strategy. This section demonstrates the onsite tests results as well as the validation test results. Discussions on the tests results are also presented.

4.1 Onsite tests of chiller critical parameters

(a) Time delay and ramping speed of chiller power

The short version of the paper was presented at ICAE2020, Dec 1-10, 2020. This paper is a substantial extension of the short version of the conference paper.

The time delay and ramping speed of power consumption in response to regulation signal is of essential importance to the frequency regulation performance. The frequency regulation capacity and performance would be overestimated if the estimated time delay is shorter than the actual value or if the system dynamics (reflected by ramping speed) is ignored. Therefore, the actual time delay and ramping speed should be discovered through onsite tests. The tests were conducted on the studied real chiller plant, and the main steps of the onsite tests is described as follows:

Step 1: Select a single chiller for the test. Set its supply chilled water temperature set-point to 5.5 °C. Set chiller power upper limit to 100%. Wait 15 minutes for the chiller to stable;

Step 2: Set the sampling period as short as possible (5 seconds in the test), and record essential data points;

Step 3: Adjust the chiller power upper limit to 75%. Record data for 10 minutes.

Step 4: Release the chiller power upper limit to 100% and end the test.

The time delay and ramping speed could be discovered based on the time series data of chiller power upper limit, chiller vane opening, and chiller power consumption. These three essential parameters are plot in a single chart and shown in Fig. 4. The chiller power limit (dashed line in Fig. 4) was changed from 100% to 75% at 19:34:15, and the vane opening (blue line in Fig. 4) began to drop significantly 20 seconds later (at 19:34:35). That means the chiller controller and chiller vane together needs about 20 seconds to respond to the change in chiller power limit settings. Prior to the change in chiller power limit, the chiller power (red line in Fig. 4) varied slightly between 1170 kW and 1190 kW. But when the vane opening dropped significantly after the change in chiller power limit (from 55.59% to 28.96%), the chiller power dropped almost instantly (from 1180 kW to 1041 kW). It took about 55 seconds (from 19:34:35 to 19:35:30) for the vane opening to change from 55.59% to 28.96%, as shown in Fig. 4(b). The

The short version of the paper was presented at ICAE2020, Dec 1-10, 2020. This paper is a substantial extension of the short version of the conference paper.

changing speed of chiller vane opening is therefore estimated to be 0.4842 %/second according to the onsite test. And the ramping speed of chiller power was 2.53 kW/s.

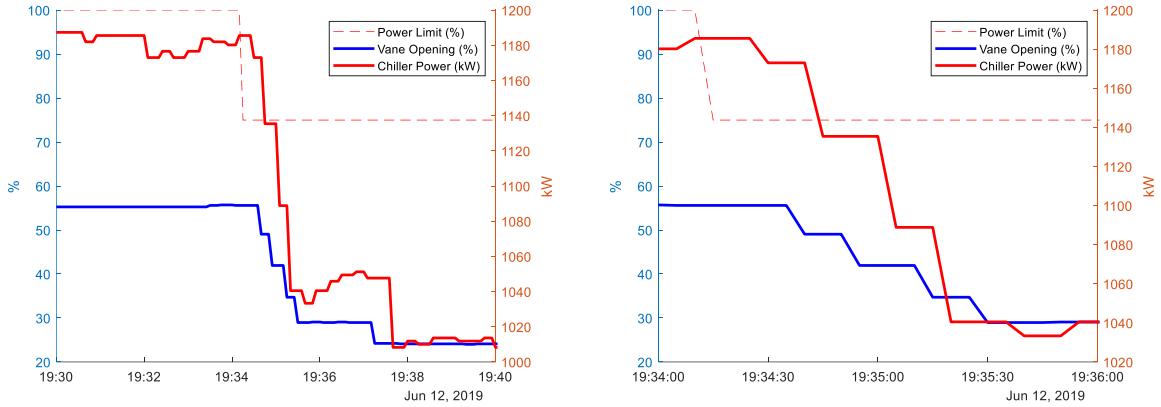

(a) Time period: 19:30 – 19:40 (b) Time period: 19:34 – 19:36

Fig. 4 Changing in chiller power upper limit, chiller vane opening, and chiller power consumption

It is noticeable that there was a variation in chiller power after 19:35:30. Because of this, the chiller local controller further reduced chiller vane opening at 19:37:15. And 25 seconds later, the chiller power reduced to 1013 kW.

As a section summary, the delay of chiller power in response to the changes in power limit settings consists of two parts. One is the delay for chiller controller to response to the power limit reset, the other is the delay for chiller power consumption to response to vane opening. Test results shown that the first part was about 20–25 seconds, while the second part was almost instant. Therefore, the overall delay time of chiller power was about 20–25 seconds. Also, the maximum changing speed of chiller vane opening was about 0.4842 %/second. The maximum ramping speed of chiller power was 2.53 kW/s.

(b) Chiller efficiency during limiting power consumption

When chiller power is limited by reducing vane opening, the chiller efficiency may be compromised. Investigation on the actual chiller efficiency during the frequency regulation is therefore needed. Fig. 5(a) shows chiller COP (Coefficient Of Performance) in the onsite test.

The short version of the paper was presented at ICAE2020, Dec 1-10, 2020. This paper is a substantial extension of the short version of the conference paper.

It is noticeable that the chiller COP reduced slightly when the vane opening was reduced. The mean COP was around 4.85 when there was no limitation on chiller power consumption (i.e. chiller power limit was 100%), and it reduced to 4.52 after chiller power limit was reset to 75%. It is also noticeable that there was a slight increase in chiller COP after chiller power limit was changed to 75%. That was because chiller COP is also affected by parameters other than chiller vane opening, such as the flow rates and temperatures of water entering condenser and evaporator.

Fig. 5(b) demonstrates the relation between chiller COP and chiller vane opening in the test. It is noticeable that the chiller efficiency increases slightly with the increase of vane opening. It can also be observed that chiller COP varies in a range rather than fixed on a certain value even if the chiller vane opening was the same. A previous study based on the same real HVAC system provides an analysis on this correlation based on data of much longer period. It was concluded that chiller efficiency could be considered high if the vane opening was higher than 40% [35].

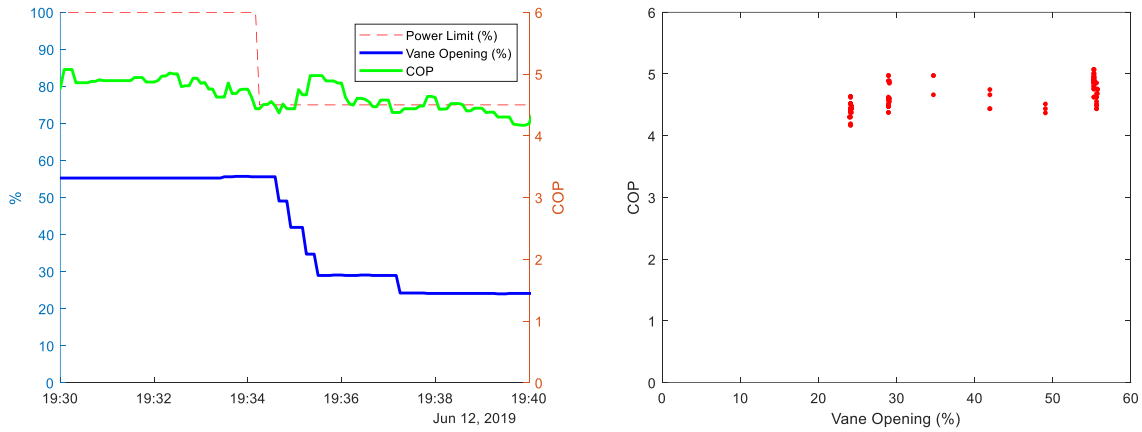

(a) Chiller COP in the power limiting test (b) Chiller COP vs Vane opening

Fig. 5 Chiller efficiency during limiting power consumption

4.2 Tests of the complete control strategy on the dynamic platform

The short version of the paper was presented at ICAE2020, Dec 1-10, 2020. This paper is a substantial extension of the short version of the conference paper.

Based on the critical parameters identified from onsite tests, the dynamic simulation platform built based on the real HVAC system is further fine-tuned. For instance, the maximum changing speed of chiller vane opening was set to 0.4842 %/second in the dynamic platform. And the minimum vane opening was set to 20% in the validation tests.

The proposed strategy for grid frequency regulation had been tested on the fine-tuned platform. Totally three chiller operation modes had been tested for comparison and evaluation. The three operation modes are (a) RegA test: Providing frequency regulation to follow the Regulation A test signals; (b) RegD test: Providing frequency regulation to follow Regulation D test signals; (c) Regular test: Not providing frequency regulation, and the chiller is controlled to always follow supply chilled water temperature set-point. In all the three test modes, the same building cooling load profile were adopted. The reference power and regulation capacity in both RegA test and RegD test were 1250 kW and 100 kW, respectively.

Table 2 shows a summary on the frequency regulation performance score in both RegA and RegD tests. The composite scores were 0.901 and 0.885 for RegA test and RegD test, respectively. The accuracy, delay and precision sub-scores for RegA test were 0.939, 0.890, and 0.872, respectively. In the RegD test, the accuracy, delay and precision sub-scores were 0.960, 0.929, and 0.765, respectively. As mentioned previously, the acceptable score for PJM frequency regulation market is 0.75. Therefore, the proposed control strategy is effective to provide grid frequency regulation using the constant speed chiller.

Table 2 Comparison on the three chiller operation modes

Test mode	Performance sub-scores			Composite score	Mean Capacity (kW)	Mean Power (kW)	Mean COP
	Accuracy	Delay	Precision				
RegA Test	0.939	0.890	0.872	0.901	6968	1216	5.73
RegD Test	0.960	0.929	0.765	0.885	6991	1254	5.57
Regular Test	NA	NA	NA	NA	7126	1267	5.62

The short version of the paper was presented at ICAE2020, Dec 1-10, 2020. This paper is a substantial extension of the short version of the conference paper.

Table 2 also shows a comparison on the chiller efficiency while providing frequency regulation. The mean COP was calculated by dividing the total capacity by the total power consumption during the entire 40 minutes tests. The chiller COP of RegA and RegD tests were 5.73 and 5.57, respectively. By comparing with the baseline (Regular test: 5.62), it is noticeable that the impact on chiller efficiency was slight.

More detailed analysis had been conducted to investigate other essential variables in the tests. Fig. 6–7 demonstrates a comparison on the target power and actual power of the chiller during the frequency regulation tests. Fig. 6 shows the data when following RegA test signal, and Fig. 7 shows the data when following RegD test signal.

It is clear that the actual power (red lines) follow the target power (blue lines) closely in both Fig. 6 and Fig. 7. It is also noticeable that the difference between the target and actual power was large whenever there was a steep change in the target power. For instance, the starting period in both RegA and RegD tests and the time period between 24 and 28 minutes in RegD test. That was because the changing speed of chiller vane opening was limited, and the chiller power had reached its maximum changing speed.

It should be mentioned that the regulation signals are continuous in practical applications, and those large power difference at the beginning of the tests would therefore be ignored (continuous tests results are shown at the end of this section). From this point of view, the chiller power could follow the target power perfectly when RegA signal was in use. However, the power difference between actual and target power could be high when RegD signal was tested, though the overall precision sub-score was still higher than acceptable.

The short version of the paper was presented at ICAE2020, Dec 1-10, 2020. This paper is a substantial extension of the short version of the conference paper.

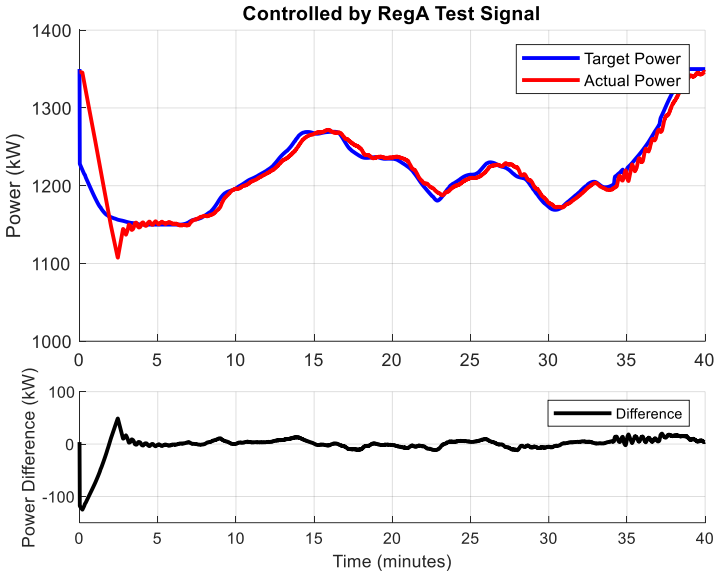

Fig. 6 Variation of chiller power in RegA Test

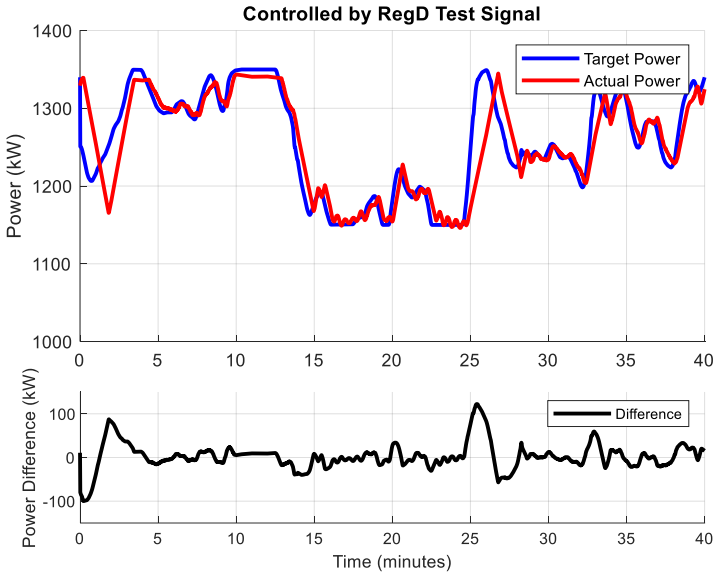

Fig. 7 Variation of chiller power in RegD Test

Further analysis was conducted to investigate the impact on building thermal environment and system efficiency when using chillers for grid frequency regulation. The chiller capacities in the three tests were compared with the building cooling load and demonstrated in Fig. 8. It can be seen that the chiller capacity varied around the building cooling load in both RegA and

The short version of the paper was presented at ICAE2020, Dec 1-10, 2020. This paper is a substantial extension of the short version of the conference paper.

RegD tests. When the chiller was in regular operation, the profile of chiller capacity followed the building cooling load profile perfectly.

Investigation on the chilled water temperature was conducted to evaluate the risk on building thermal environment. Fig. 9 shows the supply and return chilled water temperature. The variation range of supply chilled water temperature were 5.1°C–6.1°C, 5.0°C–6.1°C, and 5.4°C–5.6°C in RegA Test, RegD Test, and regular operation, respectively. The differences between maximum and minimum were about 1 K in both frequency regulation tests, while it was only 0.2 K in regular operation. That means the supply chilled water temperature had higher variation than that in regular operation. On the other hand, the variation range of return chilled water temperature were 10.1°C –11.1°C, 9.9°C –10.9°C, and 10.2°C –10.8°C in RegA Test, RegD Test, and Regular Test, respectively. The differences between maximum return temperature in regulation tests and regular operation were all only 0.3 K, which means the risk of affecting building thermal environment was extremely low.

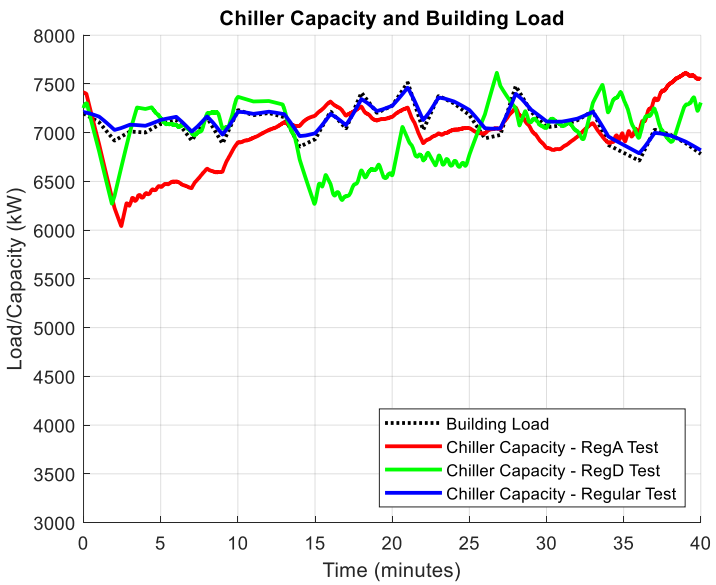

Fig. 8 Comparison on the building cooling load and chiller capacity in the three tests

The short version of the paper was presented at ICAE2020, Dec 1-10, 2020. This paper is a substantial extension of the short version of the conference paper.

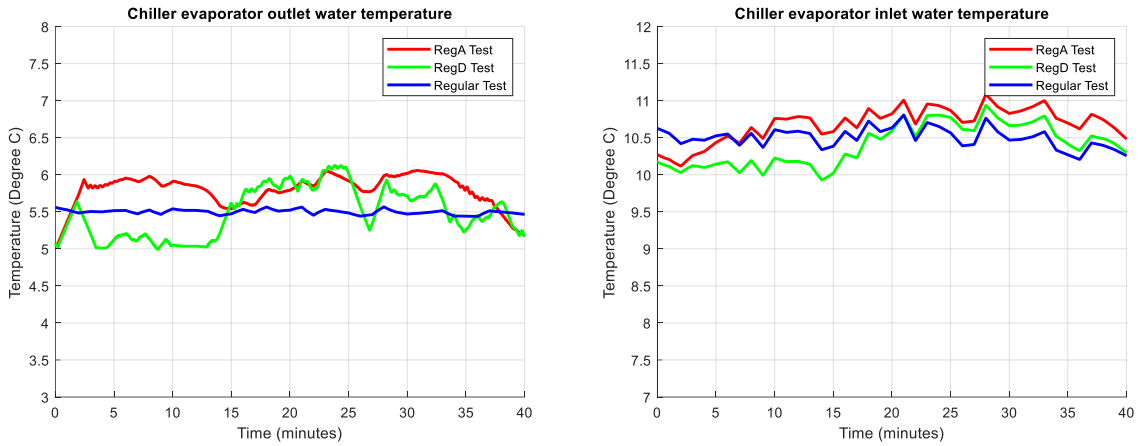

(a) Evaporator outlet water temperature (b) Evaporator inlet water temperature

Fig. 9 Comparison on the chiller water temperature in the three tests

Further tests were conducted to validate the control strategy when it is in continuous operation. The regulation signals were generated by repeating the 40 minutes test RegA and RegD signals. Both RegA and RegD tests lasted for continuous 12 hours in a working day from 8:00 to 20:00. Fig. 10 and Fig. 11 show the results of the continuous RegA test and RegD test, respectively. It can be seen that the actual chiller power strictly followed the target power in both tests. The calculated composite scores were 0.917 and 0.893 for Reg A and Reg D tests, respectively. The return chilled water temperature was always below 13 ℃, indicating that the building thermal environment could be maintained. Fig. 12 shows the chiller COP during the continuous 12 hours test. In both Reg A and Reg D tests, the chiller COP varies rapidly around the Regular test. The overall COP during the 12 hours were 5.75 in both Reg A and Reg D tests, and it was 5.74 in Regular test. Despite of the rapid variation, the impact of providing frequency regulation on the overall chiller COP could be ignored.

The short version of the paper was presented at ICAE2020, Dec 1-10, 2020. This paper is a substantial extension of the short version of the conference paper.

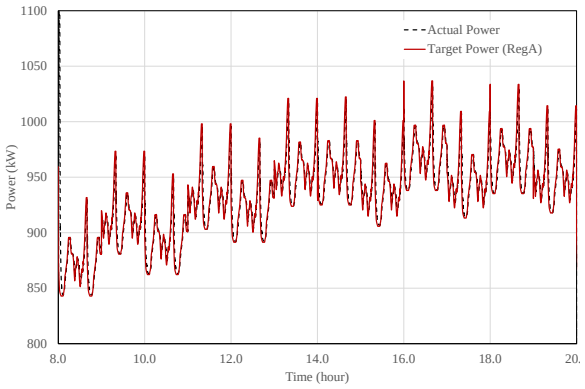

(a) Chiller power and target power

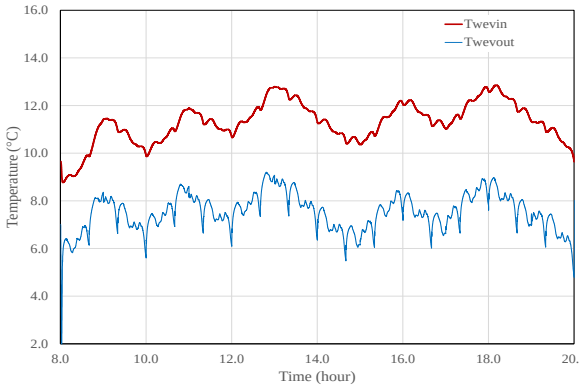

(b) Chiller water temperature

Fig. 10 RegA test for continuous 12 hours (8:00-20:00)

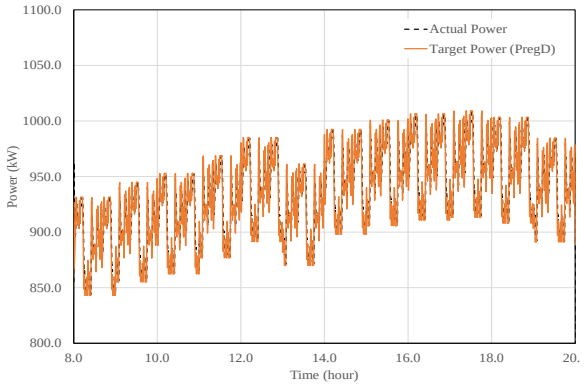

(a) Chiller power and target power

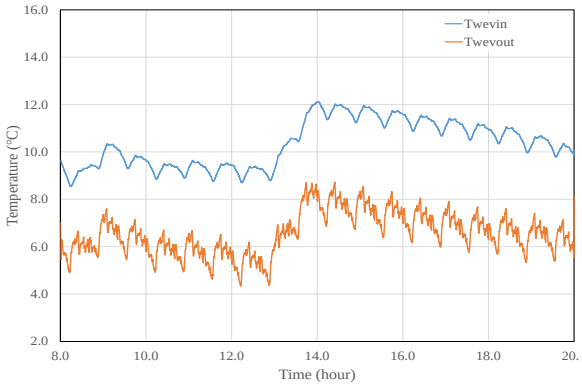

(b) Chiller water temperature

Fig. 11 RegD test for continuous 12 hours (8:00-20:00)

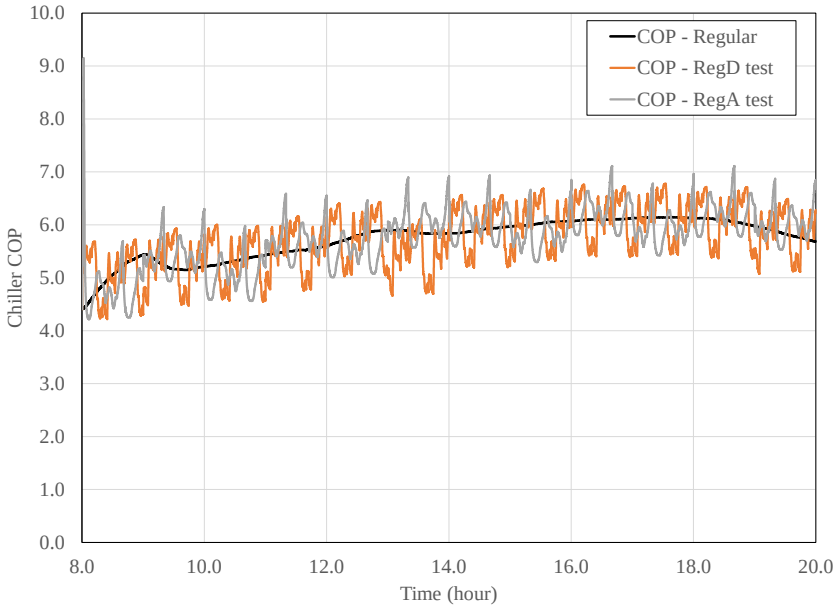

Fig. 12 Impact of providing frequency regulation on chiller COP

The short version of the paper was presented at ICAE2020, Dec 1-10, 2020. This paper is a substantial extension of the short version of the conference paper.

4.3 Further discussions on the onsite and simulation tests results

The delay time and ramping speed of chiller power affect the frequency regulation performance scores greatly. By comparison, the values discovered from the onsite tests (time delay of 20-25s) in this study indicate that the assumption in previous studies (time delay of 30s) by other researchers is close [25][26].

Simulation tests of the proposed control strategy show that a constant speed centrifugal chiller could provide frequency regulation with similar performance scores to that of using VSD chillers, by comparing with the research results presented in [29][30]. However, the regulation capacity of constant speed chiller is relatively smaller. Based on the test in this study, the constant speed centrifugal chiller could provide frequency regulation capacity of 5%-7.5% of its nominal power, while a previous research revealed that a VSD chiller could provide up to 25% of its nameplate power [29]. Considering the size of the chiller in this study, the provided frequency regulation capacity is still considerable.

5 Conclusions

With increasing penetration of intermittent renewable energy generation, the grid requires more resources for frequency regulation. Buildings thermal loads are flexible, and building thermal equipment have high potential in providing grid frequency regulation.

This study proposes a strategy to control a large constant speed centrifugal chiller for grid frequency regulation. Onsite tests were conducted in the chiller plant in a high-rise commercial building to identify critical parameters. The overall delay time of chiller power was about 20–25 seconds, and the maximum ramping speed of chiller power was 2.53 kW/s. It was also found that the overall chiller efficiency was not affected when regulating chiller power consumption. A dynamic simulation platform had been built based on the real chiller plant and fine-tuned based on the onsite tests and history data. The dynamic platform had been used to validate the

The short version of the paper was presented at ICAE2020, Dec 1-10, 2020. This paper is a substantial extension of the short version of the conference paper.

proposed control strategy. The 40 minutes Regulation A and Regulation D test signals provided by PJM were adopted in the tests. When providing 100 kW regulation capacity, the composite scores were 0.901 and 0.885 for Regulation A test and Regulation D test, respectively. It was also found that the chiller power followed the target power well when Regulation A signal was tested. But the power difference between actual and target power was higher in Regulation D test. Analysis on chiller power and chilled water temperature indicated that the chiller efficiency and building thermal environment was not affected. The continuous 12 hours regulation tests also shown that the proposed control strategy achieved high performance scores (0.917 and 0.893 for Reg A and Reg D tests, respectively) while maintaining the building thermal environment. The regulation capacity of the large constant speed chiller was 5%-7.5% of its nominal power during the continuous 12 hours test.

It should be acknowledged that the proposed control strategy is applicable for only one chiller operation. Future development will be focused on utilizing multiple chillers to provide higher frequency regulation capacity.

Acknowledgments

The research presented in this paper is financially supported by a general research grant (152079/18E) of the Research Grant Council (RGC) of Hong Kong SAR and a research grant under strategic focus area (SFA) scheme of the research institute of sustainable urban development (RISUD) in The Hong Kong Polytechnic University. The authors highly appreciate the support of Kai Shing Management Services Limited for the onsite tests.

Reference

The short version of the paper was presented at ICAE2020, Dec 1-10, 2020. This paper is a substantial extension of the short version of the conference paper.

[1] Energy Information Administration, Annual Energy Outlook 2014: with Projections to 2040, 2014.

[2] Barik AK, Jaiswal S, Das DC. Recent trends and development in hybrid microgrid: a review on energy resource planning and control. International Journal of Sustainable Energy. 2021:1-15.

[3] Energy research institute of national development and reform commission: China's renewable energy report 2020. <https://www.njwp.cn/news_2/57.html>. [Last viewed on May 27th 2021].

[4] Dong J, Attya AB, Anaya-Lara O. Provision of ancillary services by renewable hybrid generation in low frequency AC systems to the grid. International Journal of Electrical Power & Energy Systems. 2019;105:775-84.

[5] Qi Y, Dong W, Dong C, Huang C. Understanding institutional barriers for wind curtailment in China. Renewable and Sustainable Energy Reviews. 2019;105:476-86.

[6] Akram U, Nadarajah M, Shah R, Milano F. A review on rapid responsive energy storage technologies for frequency regulation in modern power systems. Renewable and Sustainable Energy Reviews. 2020;120.

[7] Buildings Energy Data Book. <http://web.archive.org/web/20130214212606/http://buildingsdatabook.eren.doe.gov/docs/DataBooks/2011_BEDB.pdf>. [Last viewed on Apr. 15th 2021].

[8] China Electricity Council. <http://www.cec.org.cn/xinwenpingxi/2017-02-09/164592.html>. [Last viewed on Apr. 15th 2021].

[9] Razmara M, Bharati GR, Hanover D, Shahbakhti M, Paudyal S, Robinett RD. Building-to-grid predictive power flow control for demand response and demand flexibility programs. Applied Energy. 2017;203:128-41.

The short version of the paper was presented at ICAE2020, Dec 1-10, 2020. This paper is a substantial extension of the short version of the conference paper.

[10] Hao H, Wu D, Lian J, Yang T. Optimal Coordination of Building Loads and Energy Storage for Power Grid and End User Services. IEEE Transactions on Smart Grid. 2018;9(5):4335-45.

[11] Fabietti L, Qureshi FA, Gorecki TT, Salzmann C, Jones CN. Multi-time scale coordination of complementary resources for the provision of ancillary services. Applied Energy. 2018;229:1164-80.

[12] Pandey SK, Mohanty SR, Kishor N. A literature survey on load–frequency control for conventional and distribution generation power systems. Renewable and Sustainable Energy Reviews. 2013;25:318-34.

[13] Wang H, Wang S, Tang R. Development of grid-responsive buildings: Opportunities, challenges, capabilities and applications of HVAC systems in non-residential buildings in providing ancillary services by fast demand responses to smart grids. Applied Energy. 2019;250:697-712.

[14] Maasoumy M. Flexibility of Commercial Building HVAC Fan as Ancillary Service for Smart Grid. 2013. <https://escholarship.org/uc/item/7hm1264j>. [Last viewed on Oct. 15th 2019].

[15] Zhao P, Henze GP, Plamp S, Cushing VJ. Evaluation of commercial building HVAC systems as frequency regulation providers. Energy and Buildings. 2013;67:225-35.

[16] Hao H, Kowli A, Lin Y, Barooah P, Meyn S. Ancillary Service for the Grid via Control of Commercial Building HVAC Systems. 2013 American Control Conference (ACC). Washington, DC, USA2013.

[17] Hao H, Lin Y, Kowli AS, Barooah P, Meyn S. Ancillary Service to the Grid Through Control of Fans in Commercial Building HVAC Systems. IEEE Transactions on Smart Grid. 2014;5(4):2066-74.

The short version of the paper was presented at ICAE2020, Dec 1-10, 2020. This paper is a substantial extension of the short version of the conference paper.

[18] Vrettos E, Kara EC, MacDonald J, Andersson G, Callaway DS. Experimental Demonstration of Frequency Regulation by Commercial Buildings—Part I: Modeling and Hierarchical Control Design. IEEE Transactions on Smart Grid. 2018;9:3213-23.

[19] Vrettos E, Kara EC, MacDonald J, Andersson G, Callaway DS. Experimental Demonstration of Frequency Regulation by Commercial Buildings—Part II: Results and Performance Evaluation. IEEE Transactions on Smart Grid. 2018;9:3224-34.

[20] Blum DH, Norford LK. Dynamic simulation and analysis of ancillary service demand response strategies for variable air volume HVAC systems. HVAC&R Research. 2014;20(8):908-21.

[21] Rotger-Griful S, Jacobsen RH, Nguyen D, Sørensen G. Demand response potential of ventilation systems in residential buildings. Energy and Buildings. 2016;121:1-10.

[22] Fu Y, Han X, Baker K, Zuo W. Assessments of data centers for provision of frequency regulation. Applied Energy. 2020;277.

[23] Wang W, Abdolrashidi A, Yu N, Wong D. Frequency regulation service provision in data center with computational flexibility. Applied Energy. 2019;251.

[24] Qureshi FA, Jones CN. Hierarchical control of building HVAC system for ancillary services provision. Energy and Buildings. 2018;169:216-27.

[25] Lin Y, Meyn SP, Barooah P. Commercial building HVAC system in power grid ancillary services. <http://plaza.ufl.edu/yashenlin/pdfs/SGC13SmartGridTech.pdf>. [Last viewed on Oct. 15th 2019].

[26] Lin Y, Barooah P, Meyn SP. Low-Frequency Power-Grid Ancillary Services From Commercial Building HVAC Systems. 2013. IEEE Smart Grid Comm 2013 Symposium - Demand Side Management, Demand Response, Dynamic Pricing.

The short version of the paper was presented at ICAE2020, Dec 1-10, 2020. This paper is a substantial extension of the short version of the conference paper.

[27] Cai J, Braun JE. Laboratory-based assessment of HVAC equipment for power grid frequency regulation: Methods, regulation performance, economics, indoor comfort and energy efficiency. Energy and Buildings. 2019;185:148-61.

[28] Cai J, Braun JE. A regulation capacity reset strategy for HVAC frequency regulation control. Energy and Buildings. 2019;185:272-86.

[29] Su L, Norford LK. Demonstration of HVAC chiller control for power grid frequency regulation—Part 1: Controller development and experimental results. Science and Technology for the Built Environment. 2015;21(8):1134-42.

[30] Su L, Norford LK. Demonstration of HVAC chiller control for power grid frequency regulation—Part 2: Discussion of results and considerations for broader deployment. Science and Technology for the Built Environment. 2015;21(8):1143-53.

[31] Sumathi S, Kumar LA, Surekha P. Solar PV and wind energy conversion systems. Switzerland: Spriger; 2015. 2015.

[32] Shan K, Fan C, Wang J. Model predictive control for thermal energy storage assisted large central cooling systems. Energy. 2019;179:916-27.

[33] Hui H, Ding Y, Song Y, Rahman S. Modeling and control of flexible loads for frequency regulation services considering compensation of communication latency and detection error. Applied Energy. 2019;250:161-74.

[34] PJM Manual 12: Balancing Operations. <https://www.pjm.com/~/media/documents/manuals/m12.ashx>. [Last viewed on Apr. 15th 2021].

[35] Shan K, Wang S, Gao D-c, Xiao F. Development and validation of an effective and robust chiller sequence control strategy using data-driven models. Automation in Construction. 2016;65:78-85.

The short version of the paper was presented at ICAE2020, Dec 1-10, 2020. This paper is a substantial extension of the short version of the conference paper.

[36] Shan K, Wang S, Tang R. Direct chiller power limiting for peak demand limiting control in buildings—Methodology and on-site validation. Automation in Construction. 2018;85:333-43.

[37] Zhu N, Shan K, Wang S, Sun Y. An optimal control strategy with enhanced robustness for air-conditioning systems considering model and measurement uncertainties. Energy and Buildings. 2013;67:540-50.

[38] Klein, S.A. et al., 2017, TRNSYS 18: A Transient System Simulation Program, Solar Energy Laboratory, University of Wisconsin, Madison, USA, <http://sel.me.wisc.edu/trnsys>. [Last viewed on Apr. 15th 2021].

[39] S.W. Wang, J.B. Wang, J. Burnett, Mechanistic model of centrifugal chillers for HVAC system dynamics simulation, Build. Serv. Eng. Res. Technol. 21 (2000) 73–83.

The short version of the paper was presented at ICAE2020, Dec 1-10, 2020. This paper is a substantial extension of the short version of the conference paper.